AIP Advances

Electron spin resonance in a proximity-coupled MoS_2/graphene van der Waals heterostructure

Cite as: AIP Advances **12**, 035111 (2022); https://doi.org/10.1063/5.0077077
Submitted: 06 December 2021 • Accepted: 15 February 2022 • Published Online: 03 March 2022

Chithra H. Sharma, Pai Zhao, Lars Tiemann, et al.

Electron spin resonance in a proximity-coupled MoS_2/graphene van der Waals heterostructure

Cite as: AIP Advances 12, 035111 (2022); doi: 10.1063/5.0077077
Submitted: 6 December 2021 • Accepted: 15 February 2022 •
Published Online: 3 March 2022

Chithra H. Sharma,[1,a)] Pai Zhao,[1,2] Lars Tiemann,[1] Marta Prada,[3] Arti Dangwal Pandey,[4] Andreas Stierle,[1,4] and Robert H. Blick[1,5,b)]

AFFILIATIONS

[1] Center of Hybrid Nanostructures (CHyN), Department of Physics, Universität Hamburg, Luruper Chaussee 149, 22761 Hamburg, Germany
[2] Institute of Microsystems Technology, Hamburg University of Technology, 21703 Hamburg, Germany
[3] Institute for Theoretical Physics, Universität Hamburg, HARBOR, Luruper Chaussee 149, 22761 Hamburg, Germany
[4] Centre for X-ray and Nano Science CXNS, Deutsches Elektronen-Synchrotron DESY, Hamburg, Germany
[5] Materials Science and Engineering, University of Wisconsin-Madison, University Ave. 1550, Madison, Wisconsin 53706, USA

[a)] **Author to whom correspondence should be addressed:** Chithra.Sharma@physik.uni-hamburg.de
[b)] **Electronic mail:** rblick@physnet.uni-hamburg.de

ABSTRACT

Coupling graphene's excellent electron and spin transport properties with a higher spin–orbit coupling (SOC) material allows tackling the hurdle of spin manipulation in graphene due to the proximity to van der Waals layers. Here, we use magneto-transport measurements to study the electron spin resonance on a combined system of graphene and MoS_2 at 1.5 K. The electron spin resonance measurements are performed in the frequency range of 18–33 GHz, which allows us to determine the g-factor in the system. We measure the average g-factor of 1.91 for our hybrid system, which is a considerable shift compared to that observed in graphene on SiO_2. This is a clear indication of proximity induced SOC in graphene in accordance with theoretical predictions.

Proximity causes interaction—naturally, this basic rule also holds for nanoscale junctions made of van der Waals (vdW) materials.[1,2] By now, it is possible to assemble a large number of different vdW materials in order to tailor a system with specific properties, thus bringing together the best of "many worlds." In particular, hexagonal boron nitride (h-BN) has been used to encapsulate vdW materials, enhancing the electronic properties of graphene (Gr) as well as different transition metal dichalcogenides (TMDCs).[1,2] For MoS_2 and WS_2, this has been studied in p–n junctions via excitons[3] and in twisted homo-bilayers,[4,5] which show correlated electronic phases. MoS_2 and Gr are heavily studied systems individually. While Gr is a semi-metal, MoS_2 is a semiconductor (intrinsically typically n-doped) with large spin–orbit coupling (SOC), where the carrier density and thus its conductivity can be tuned by means of a gate voltage. The mobility and conductivity of MoS_2, however, are limited predominantly due to the rough interface and the SiO_2 substrates. In addition, it forms Schottky contacts with most metals, so that the fabrication of Ohmic contacts is a challenge.[6] On the other hand, Gr is well studied as a Dirac metal with high charge carrier conductivity and mobility,[7] but its device performance has been limited due to the lack of a bandgap and relatively small intrinsic SOC of the order of only 40 μeV.[8–11] Enhancing the SOC with TMDCs in close proximity is thus a way to marry the benefits of the properties of both materials.

Graphene can be employed as an Ohmic contact (or conductive backbone) material for MoS_2.[12,13] It is assumed that valley-Zeeman and Rashba-SOC are induced in Gr-on-TMDCs via the proximity effect.[14–18] Furthermore, it was suggested that the bandgap of MoS_2 could be tuned in Gr/MoS_2 heterostructures.[19] This induced SOC is expected to be up to two orders of magnitude higher than the intrinsic value of Gr. In accordance with this, proximity induced SOC has been reported in a few experimental studies for heterostructures of Gr/WS_2,[20,21] Gr/WSe_2,[18] and Gr/MoS_2.[18,22] Proximity induced spin lifetime anisotropy has also been explored in Gr/TMDC($MoSe_2$).[23,24] So far, the signatures of induced SOC have been observed via magneto-transport embedded in weak anti-localization (WAL)[18,21] measurements, or via the spin Hall effect,[20,22] in Coulomb-drag effect studies,[25] and in the modulation of the Schottky barrier height.[26] Among these, only a couple of studies reported the electron transport behavior in Gr-on-MoS_2 at low temperatures.[18,25] A direct measurement of the g-factor on such a hybrid system has not been performed until today. Here, the premise is that the g-factor for free electrons is well-known with a value of 2.0023.[27,28] Any deviation is an indication of SOC in the system. In previous resistively detected electron spin resonance (ESR) measurements on single-layer and multi-layer Gr, a g-factor, parallel to the c axis of (1.952 ± 0.002), was determined for Gr-on-SiO_2.[29]

Here, we report on a detailed resistively detected ESR traced in magneto-transport of Gr-on-MoS_2 (or in short GroMoS) samples in direct comparison with standard Gr-on-SiO_2 (or GroSi). The four-point measurements of the electrical resistance of the device are carried out at 1.5 K, as shown in the schematic architecture in Fig. 1(a). In order to couple an ESR signal, a Hertzian resonator coil is placed in the vicinity of the sample for microwave irradiation, which will be discussed in the following.[29] The magnetic field component of the microwave ($\boldsymbol{B}_\nu$) has to be perpendicular to the external magnetic field ($\boldsymbol{B}$).[30] The magnetic moment of the electron precesses around the direction of $\boldsymbol{B}$, while a resonant $\boldsymbol{B}_\nu$ tips the magnetic moment into the plane, i.e., perpendicular direction to $\boldsymbol{B}$. In terms of energy, the spin energy level splits with $\boldsymbol{B}$, while $\boldsymbol{B}_\nu$ causes spin flips when the frequency matches the splitting, according to the equation $h\nu = g\mu_B B$. These resonant spin flips are observed as a change in the resistance attributed to spin energy being transferred to mobile electrons and momentum randomization of electrons.[31–33]

We use standard magneto-transport measurements to detect ESR, evaluate the charge transfer between the layers, and determine the doping density. We are able to report on the deviation of the g-factor ($g \parallel$ c axis) of Gr from its intrinsic value in the heterostructure signaling that the SOC is altered by the close proximity of the MoS_2 layer.

We exfoliated few-layer MoS_2 on a 300 nm SiO_2/Si wafer and fabricated a Hall-bar of CVD-grown Gr (Graphenea Semiconductor S.L., Spain) on top.[29,34] A part of the Gr Hall-bar covers the MoS_2 sample, while the other part is directly placed on SiO_2, as shown in Fig. 1(b). The contacts were fabricated on top of the Gr on both regions using standard electron beam lithography techniques with Ti/Au (4/70 nm) metallization. Figure 1(b) shows the optical image of the device where the exfoliated MoS_2 flake is outlined by the purple dotted line as a guide to the eye. The reactive ion etching process for the Hall-bar fabrication (also etched the MoS_2 outside the defined region) ensures Ohmic contacts on Gr. The highly p-doped Si under a 300 nm thick SiO_2 dielectric was used as the gate electrode to tune the carrier concentration.

In order to characterize GroSi and GroMoS, we performed Raman spectroscopy with a standard 532 nm laser, as shown in Figs. 1(c) and 1(d). Figure 1(c) shows the peaks corresponding to MoS_2 where the in-plane (E^1_{2g}) and out-of-plane vibration peaks (A_{1g}) are observed at 383.8 and 408.6 cm^{-1}, respectively, only on the GroMoS. Clear G and 2D peaks of Gr are observed in both the regions in Fig. 1(d). We do not observe any significant D-peak, indicating that the quality of Gr has not been compromised. We observe that GroMoS shows a small upshift in the 2D peak position compared to GroSi. The observed upshift is consistent with the vdW interaction with the MoS_2 flake.[35] Atomic force microscopy (AFM) performed on the sample after the transport measurements reveals that the uniformity of the graphene layer on MoS_2 has not been

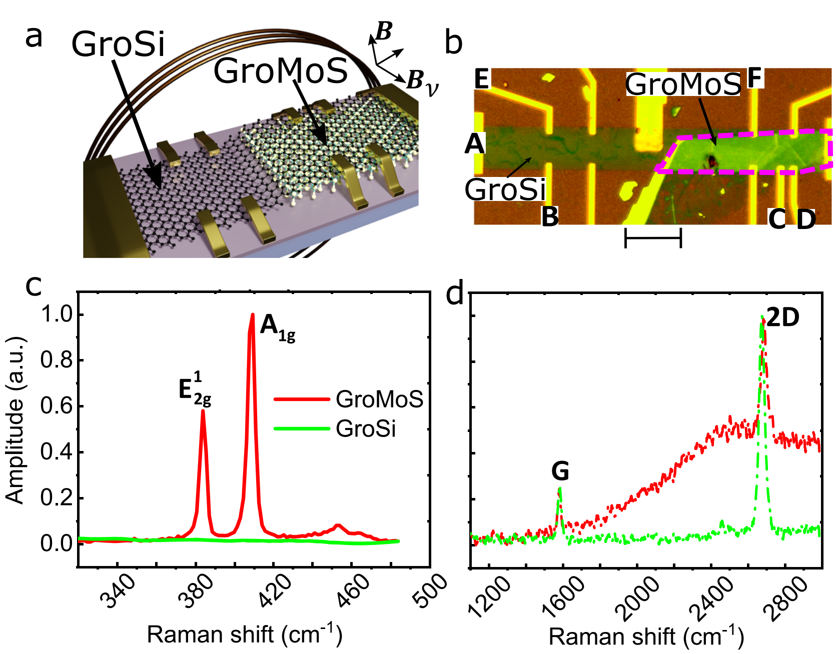

FIG. 1. (a) Schematic representation of the device architecture including the Hertzian-loop antenna for coupling the microwave signal for ESR. (b) Optical image of the device: the dotted purple region traces the outline of the MoS_2 flake. The contacts used for the measurements are labeled as A–F. The scale bar is 20 μm. (c) and (d) The Raman spectra taken from the GroMoS and GroSi regions are shown in red and green, respectively. (c) E^1_{2g} and A_{1g} peaks of MoS_2 (d) G and 2D peaks of Gr as dotted lines (see text for details).

compromised (see the supplementary material, Fig. S1). The thickness of the flakes measured by AFM is higher than those attributed to the moisture adsorption and thermal cycling.

The device was annealed after fabrication at 200 °C in vacuum of 10^{-4} mbar overnight to remove any excess moisture.[34] The sample was then cooled to 1.5 K in a helium bath cryostat without breaking the vacuum. All transport measurements shown are performed at 1.5 K with and without a perpendicular magnetic field. The results to be discussed further are measured in four-point lock-in configuration by passing an AC current across the probes marked as A and D (ground) of Fig. 1(a).

Figure 2(a) shows the longitudinal resistance of the device measured between probes B and C as a function of the applied back gate voltage (V_g). This measurement was performed over the whole Gr Hall-bar where one voltage probe is on GroSi and the other on GroMoS. The black and green dotted line traces show the forward and backward sweep, respectively, where a clear ambipolar behavior is observed, as expected in Gr. The solid traces are respective Lorentzian fits to the measured transresistance. The charge neutrality point (CNP) for the Gr is $V_g \sim 7$ V. The doping of the graphene is appreciably small, and we do not observe a significant hysteresis, which would be indicative of reduced moisture on the sample.[34]

As observed commonly for CVD-grown Gr, we find weak localization (WL) signatures as a result of the strong inter-valley scattering.[36] WL is observed for all gate voltages with the data close to the CNP shown in Fig. 2(b). The Hall resistance measured across probes B and E for different gate voltages is shown in Fig. 2(c). Note that this Hall measurement is performed in the GroSi region alone. The sign reversal of the slope between 7 and 8 V signals the change in the carrier type from holes to electrons at the CNP. We also observe a small WL peak in the Hall data from a small parasitic longitudinal component in the measurement. The Hall slope is plotted against the gate voltage in Fig. 2(d), where the sign change is most evident. The mobility of the Gr is estimated to be ~500 $cm^2\ V^{-1}\ s^{-1}$. The poor mobility in the device could be a result of the grain boundaries and wrinkles in our samples as observed in the AFM image (supplementary material, Fig. S1).[37]

The carrier density is calculated close to the CNP using a two-carrier model[38] (for details, see supplementary material S2) and plotted in Fig. 2(e) using the longitudinal and transverse resistances in Figs. 2(b) and 2(c), respectively. The blue open circles and red filled circles represent the holes and electrons, respectively. The blue and red lines are linear fits to the carrier density that is lowest around ~ 8 V. We also note a small asymmetry in the change of carrier density with the gate voltage for the hole and the electron side. We attribute this to the GroMoS region in the device. A saturation of the electron carrier density has been observed previously in GroMoS devices as a result of the negative compressibility in the system.[39]

From a separate measurement on the GroMoS region (see the supplementary material, Fig. S2), we observe that the CNP is shifted to ~−6 V, implying that MoS_2 is n-doping the Gr and thus a strong interaction between the systems is induced. We also observe jumps in the I–V characteristics taken from the GroMoS region as opposed to the whole sample, which is indicative of an exchange of electrons between the two layers (supplementary material, Fig. S3). We do not observe any ESR from this region, presumably as the cross

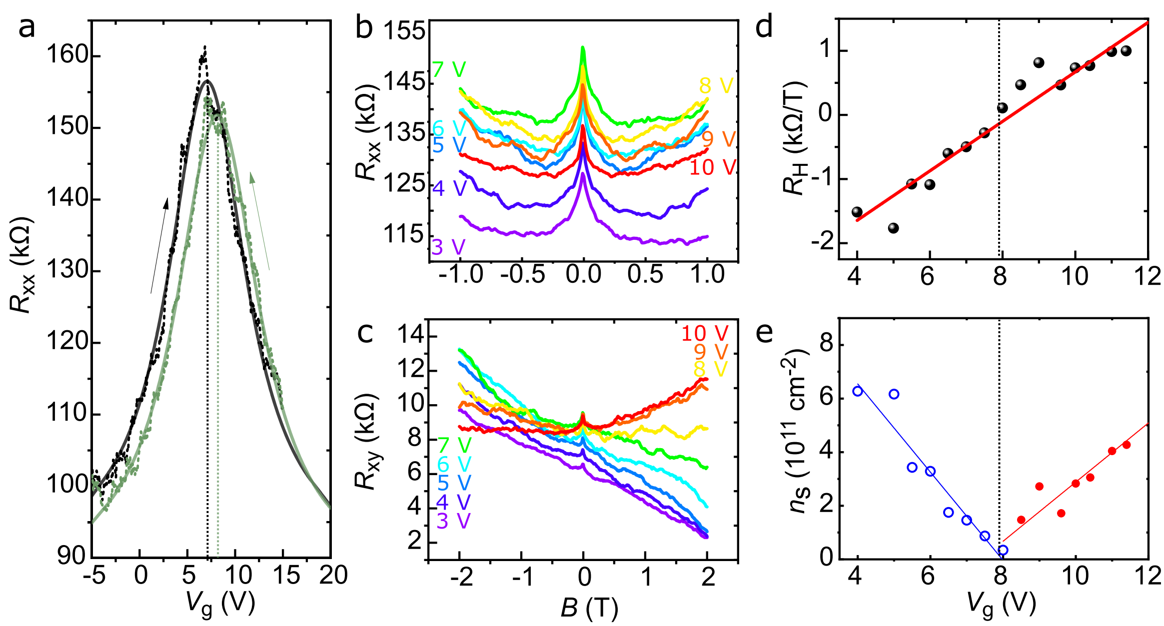

FIG. 2. (a) Transresistance of the device measured across B and C, which is sampling over the Gr covering SiO_2 as well as the MoS_2. The black and green traces show forward and backward sweeps, respectively, in dotted lines, while the full lines show Lorentzian fits to the data. (b) and (c) Magneto-transport of the device at different gate voltages measured between contacts (b) B and C showing weak localization and (c) B and E showing the Hall resistance. The gate voltages are indicated by the color scale in the graphs. (d) Variation of the Hall slope as a function of gate voltage close to the CNP, indicating that we are dealing with a hole-carrier system in total. (e) Carrier density as a function of gate voltage close to the CNP calculated based on the two-carrier model (see supplementary material S1 for details).

section of the probed region is too small to induce a measurable signal.

Proximity induced SOC interactions between Gr and MoS_2 are reflected in the electronic *g*-factor, which we can experimentally address via ESR. Here, the magneto-resistance is measured across contacts B and C while simultaneously applying microwave radiation using a Hertzian coil antenna, as shown in the schematic in Fig. 1(a). The resonance signal is observed in the difference ΔR_{xx} of the magneto-transport measurements with and without radiation (dark), $\Delta R_{xx}(B, h\nu) = R_{xx}(B, h\nu) - R_{xx}(B, dark)$. The signal peak follows the resonance condition $h\nu = g\mu_B B$ corresponding to the Zeeman splitting for various microwave frequencies ν.[40]

Figure 3(a) shows exemplary traces of ΔR_{xx}, measured at a gate voltage of 6.1 V, with ESR peaks highlighted by a dotted line as a guide to the eye. The smaller non-dispersive peak centered at $B = 0$ is an artifact from the temperature dependence of WL under non-resonant heating. The dense color-scale plot in Fig. 3(b) is a summary of all frequencies. The resonance region is marked with a magenta dashed line. Figure 3(c) shows a linear fit of the resonance, where the slope reflects the g-factor at 6.1 V. Similarly, we are now able to extract the *g*-factor for all other gate voltages around the CNP. The result of this *g*-factor analysis is plotted in Fig. 3(d) over the gate voltage range of interest. A detailed inspection results in an average value of 1.91 (red dashed line) as opposed to earlier reports on pure Gr, which reported a constant value of 1.952 ± 0.002, irrespective of the gate voltage.[10,29] We also calculated the spin lifetime using $\tau_s = \hbar/2\Delta E \cong (71.5 \pm 4)$ ps, where $\Delta E = \mu_B \Delta B$ is the Zeeman energy and ΔB is the half width of the ESR peaks.[29] This is comparable to the reported out-of-plane spin lifetime values for graphene and Gr/TMDC.[23,29] The half width (spin lifetime) is slightly smaller (larger) in comparison to that measured in GroSi reported by Lyon *et al.*[29] The graphene flake in our device lies partly over MoS_2. We believe this lowers the electron–hole puddles caused by the SiO_2 substrate, thereby increasing the spin lifetime.[41]

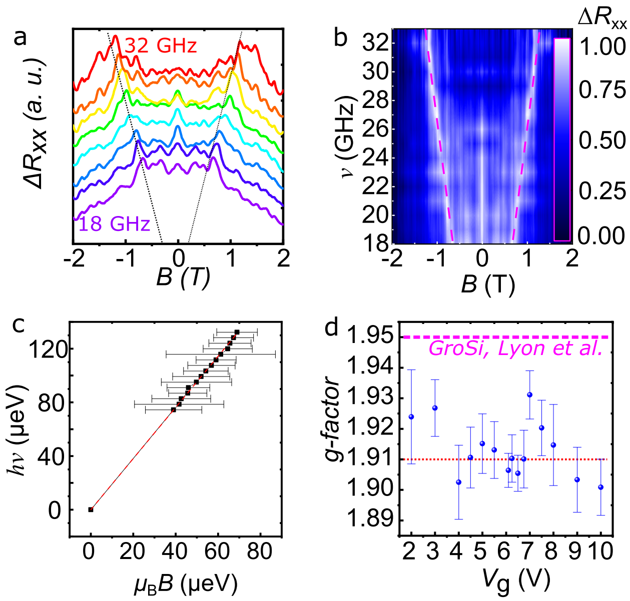

FIG. 3. (a) Magneto-transport of the device between contacts B and C under microwave radiation at V_g = 6.1 V. Plotted is ΔR_{xx}, as the difference in magnetoresistance with and without continuous microwave radiation. The ESR signal is clearly discernible, dispersing linearly (dotted lines) with frequency from 18 to 32 GHz. (b) Color-scale plot of the detailed frequency dependence. The plots are normalized for clarity. The resonance is marked with magenta dashed lines. (c) Analysis of all ESR data for V_g = 6.1 V revealing spin resonance (fits are anchored at zero). (d) Extracted *g*-factor of all ESR data over the gate voltage range of interest next to the CNP. The average value is marked with the red dashed line, and the measured value for graphene on SiO_2 from Ref. 29 is marked with the magenta dashed line (see text for details).

In contrast to former measurements, we observe a strong variation of the *g*-factor with gate voltage (i.e., carrier concentration). For positive V_g, the *g*-factor correction is twice as large as that for pure Gr,[29] which is consistent with the SOC enhancement via the proximity effect. As described by Gmitra and Fabian,[16] a positive electric field induces a carrier transfer between graphene and MoS_2, where first principle calculations estimate a splitting of ~1 meV. Hence, we can assume that the *g*-factor variation from 1.95 to 1.91 and its dependence on the gate voltage are proximity-induced, signaling the interaction with the MoS_2 layers. We stress that the measurement was carried out over a large strip of Gr covering SiO_2 as well as MoS_2. This "mixed" approach was necessary to improve the signal-to-noise ratio in ΔR_{xx}. We have not been able to obtain a recognizable ESR signal when the distance between the voltage probes is reduced. This, we assume, is due to the smaller number of spin flips owing to smaller area.

In conclusion, we can state that a clear ESR signal in the heterostructure of Gr/MoS_2 is traceable due to the interaction between the two systems. Variations of the *g*-factor indicate crosstalk of the strong spin–orbit coupled electrons of MoS_2 to the carriers in Gr as expected from theoretical calculations.[14–18] Enhanced SOC in Gr can potentially lead to topological phases, such as the quantum spin Hall effect.[11] Understanding the exact nature of this coupling will enable us to design spin-transfer devices with possibly extremely enhanced spin-relaxation times.

SUPPLEMENTARY MATERIAL

See the supplementary material for the AFM image of the device, description of the two-carrier model for graphene, transresistance measurement in the GroMoS region, and *I–V* characteristics.

ACKNOWLEDGMENTS

This work was supported in the early stages by the Center for Excellence Advanced Imaging of Matter (AIM) of the Deutsche Forschungsgemeinschaft (DFG) under Grant No. EXC-2056 and the Partnership for Innovation Education and Research (PIER) under Grant No. PIF-2021-01. We acknowledge direct support by the Alexander von Humboldt Foundation for C. H. Sharma. We thank Professor H. P. Oepen for discussions on spin transport. We thank Jann Harberts for the help and suggestions on the schematics. All measurements in this work were performed with NANOMEAS. R.H.B. would like to thank Alberto F. Morpurgo for enlightening discussions on the prospects of vdW materials.

AUTHOR DECLARATIONS

Conflict of Interest

The authors have no conflicts to disclose.

DATA AVAILABILITY

The data that support the findings of this study are available from the corresponding author upon reasonable request.

REFERENCES

[1] K. S. Novoselov, A. K. Geim, S. V. Morozov, D. Jiang, Y. Zhang, S. V. Dubonos, I. V. Grigorieva, and A. A. Firsov, Science **306**, 666 (2004).
[2] K. S. Novoselov, A. Mishchenko, A. Carvalho, and A. H. Castro Neto, Science **353**, aac9439 (2016).
[3] S. Gao, L. Yang, and C. D. Spataru, Nano Lett. **17**, 7809 (2017).
[4] Y. Cao, V. Fatemi, A. Demir, S. Fang, S. L. Tomarken, J. Y. Luo, J. D. Sanchez-Yamagishi, K. Watanabe, T. Taniguchi, E. Kaxiras, R. C. Ashoori, and P. Jarillo-Herrero, Nature **556**, 80 (2018).
[5] F. Wu, T. Lovorn, E. Tutuc, I. Martin, and A. H. Macdonald, Phys. Rev. Lett. **122**, 086402 (2019).
[6] C. Gong, L. Colombo, R. M. Wallace, and K. Cho, Nano Lett. **14**, 1714 (2014).
[7] A. K. Geim and K. S. Novoselov, Nat. Mater. **6**, 183 (2007).
[8] M. Gmitra, S. Konschuh, C. Ertler, C. Ambrosch-Draxl, and J. Fabian, Phys. Rev. B **80**, 235431 (2009).
[9] J. Sichau, M. Prada, T. Anlauf, T. J. Lyon, B. Bosnjak, L. Tiemann, and R. H. Blick, Phys. Rev. Lett. **112**, 046403 (2019).
[10] R. G. Mani, J. Hankinson, C. Berger, and W. A. De Heer, Nat. Commun. **3**, 996 (2012).
[11] C. L. Kane and E. J. Mele, Phys. Rev. Lett. **95**, 226801 (2005).
[12] L. Wang, I. Meric, P. Y. Huang, Q. Gao, Y. Gao, H. Tran, T. Taniguchi, K. Watanabe, L. M. Campos, D. A. Muller, J. Guo, P. Kim, J. Hone, K. L. Shepard, and C. R. Dean, Science **342**, 614 (2013).
[13] M. Houssa, K. Iordanidou, A. Dabral, A. Lu, R. Meng, G. Pourtois, V. V. Afanas'ev, and A. Stesmans, Appl. Phys. Lett. **114**, 163101 (2019).
[14] A. David, P. Rakyta, A. Kormányos, and G. Burkard, Phys. Rev. B **100**, 085412 (2019).
[15] J. H. Garcia, A. W. Cummings, and S. Roche, Nano Lett. **17**, 5078 (2017).
[16] M. Gmitra and J. Fabian, Phys. Rev. B **92**, 155403 (2015).
[17] Z. Wang, D. K. Ki, J. Y. Khoo, D. Mauro, H. Berger, L. S. Levitov, and A. F. Morpurgo, Phys. Rev. X **6**, 041020 (2016).
[18] B. Yang, M. Lohmann, D. Barroso, I. Liao, Z. Lin, Y. Liu, L. Bartels, K. Watanabe, T. Taniguchi, and J. Shi, Phys. Rev. B **96**, 041409 (2017).
[19] A. Ebnonnasir, B. Narayanan, S. Kodambaka, and C. V. Ciobanu, Appl. Phys. Lett. **105**, 031603 (2014).
[20] A. Avsar, J. Y. Tan, T. Taychatanapat, J. Balakrishnan, G. K. W. Koon, Y. Yeo, J. Lahiri, A. Carvalho, a. S. Rodin, E. C. T. O'Farrell, G. Eda, A. H. Castro Neto, and B. Özyilmaz, Nat. Commun. **5**, 4875 (2014).
[21] Z. Wang, D. K. Ki, H. Chen, H. Berger, A. H. MacDonald, and A. F. Morpurgo, Nat. Commun. **6**, 8339 (2015).
[22] C. K. Safeer, J. Ingla-Aynés, F. Herling, J. H. Garcia, M. Vila, N. Ontoso, M. R. Calvo, S. Roche, L. E. Hueso, and F. Casanova, Nano Lett. **19**, 1074 (2019).
[23] T. S. Ghiasi, J. Ingla-Aynés, A. A. Kaverzin, and B. J. Van Wees, Nano Lett. **17**, 7528 (2017).
[24] A. W. Cummings, J. H. Garcia, J. Fabian, and S. Roche, Phys. Rev. Lett. **119**, 206601 (2017).
[25] Y. Jin, M.-K. Joo, B. H. Moon, H. Kim, S. Lee, H. Y. Jeong, and Y. H. Lee, Commun. Phys. **3**, 189 (2020).
[26] C.-J. Shih, Q. H. Wang, Y. Son, Z. Jin, D. Blankschtein, and M. S. Strano, ACS Nano **8**, 5790 (2014).
[27] B. Odom, D. Hanneke, B. D'urso, and G. Gabrielse, Phys. Rev. Lett. **97**, 030801 (2006).
[28] G. Gabrielse, D. Hanneke, T. Kinoshita, M. Nio, and B. Odom, Phys. Rev. Lett. **97**, 030802 (2006).
[29] T. J. Lyon, J. Sichau, A. Dorn, A. Centeno, A. Pesquera, A. Zurutuza, and R. H. Blick, Phys. Rev. Lett. **119**, 066802 (2017).
[30] C. P. Slichter, *Principles of Magnetic Resonance*, 3rd ed. (Harper & Row Publishers, New York, 1963).
[31] S. Toyotomi, J. Phys. Soc. Jpn. **37**, 130 (1974).
[32] K. Morigaki and M. Onda, J. Phys. Soc. Jpn. **36**, 1049 (1974).
[33] N. Singh and L. Rani, J. Magn. Magn. Mater. **474**, 501 (2019).
[34] T. J. Lyon, J. Sichau, A. Dorn, A. Zurutuza, A. Pesquera, A. Centeno, and R. H. Blick, Appl. Phys. Lett. **110**, 113502 (2017).
[35] K.-G. Zhou, F. Withers, Y. Cao, S. Hu, G. Yu, and C. Casiraghi, ACS Nano **8**, 9914 (2014).
[36] F. V. Tikhonenko, D. W. Horsell, R. V. Gorbachev, and A. K. Savchenko, Phys. Rev. Lett. **100**, 056802 (2008).
[37] H. S. Song, S. L. Li, H. Miyazaki, S. Sato, K. Hayashi, A. Yamada, N. Yokoyama, and K. Tsukagoshi, Sci. Rep. **2**, 337 (2012).
[38] M. J. Kane, N. Apsley, D. A. Anderson, L. L. Taylor, and T. Kerr, J. Phys. C: Solid State Phys. **18**, 5629 (1985).
[39] S. Larentis, J. R. Tolsma, B. Fallahazad, D. C. Dillen, K. Kim, A. H. Macdonald, and E. Tutuc, Nano Lett. **14**, 2039 (2014).
[40] D. Stein, K. V. Klitzing, and G. Weimann, Phys. Rev. Lett. **51**, 130 (1983).
[41] D. Van Tuan, F. Ortmann, A. W. Cummings, D. Soriano, and S. Roche, Sci. Rep. **6**, 21046 (2016).